Research Article

Comparative study of the electrochemical properties of $P4_332$ and Fd3m space group of $LiNi_{0.45}Cu_{0.05}Mn_{1.5}O_4$ cathode materials

Miao-Miao Deng[1,2] · Da-Wei Zhang[1] · Aqsa Yasmin[2] · Jia-Ying Liao[2] · Xiao-Dong He[2] · Chun-Hua Chen[2]

Abstract
The $LiNi_{0.45}Cu_{0.05}Mn_{1.5}O_4$ cathode materials with two different space groups $P4_332$ and Fd3m are synthesized via a thermopolymerization method followed by different calcination processes. The results demonstrate that $LiNi_{0.45}Cu_{0.05}Mn_{1.5}O_4$ cathode material with Fd3m space group offers much better electrochemical performances than the one with $P4_332$ space group. The sample with Fd3m space group delivers specific capacities of 118.7 and 110.4 mAh g^{-1} at 8 C and 10 C rates, respectively. Furthermore, it also offers excellent cycling stability at room temperature with the capacity retention 91.2% after 500 cycles. Even at the elevated temperature (55 °C), its capacity retention can still remain 100% after 100 cycles. All these indicate that $LiNi_{0.45}Cu_{0.05}Mn_{1.5}O_4$ cathode material with Fd3m space group has a great potential in the application of the large-scale electronic devices.

Keywords Lithium-ion battery · Copper doping · Lithium nickel manganese oxide · A thermopolymerization method

1 Introduction

With the energy and environment challenges, the lithium-ion battery as a preferred second battery is highly demanded for the portable electronic devices and even the large-scale applications due to its higher power density, safety, low cost and environmental friendliness [1–3]. Moreover, with the rapid development of the electronic devices and automobile industry, the lithium batteries are required to supply a longer cycling life, higher energy density and superior security. In this case, the 5 V spinel $LiNi_{0.5}Mn_{1.5}O_4$ cathode comes into the sight of people and also attracts much more attentions for its high energy density of 640 W h kg^{-1}, good cycling capability and rate performance at room temperature [4–8].

However, the shortcomings of the spinel $LiNi_{0.5}Mn_{1.5}O_4$ material seriously restrict its commercial applications, which include the decomposition of electrolyte at high working voltage, the sharp capacity fading at high temperature (50–60 °C), and poor rate performance [6, 8, 9]. Partial substitutions at Ni site or Mn site in $LiNi_{0.5}Mn_{1.5}O_4$ with different metal ions such as Fe, Co, Cr, Al, Mg, Cu, Ru, Ti, Nb etc. [4, 10–21] have proved to be an effective way to improve its electrochemical properties. On the other hand, the structures of spinel $LiNi_{0.5}Mn_{1.5}O_4$ belong to two different space groups, a face-centered cubic Fd3m space group with Ni^{2+} and Mn^{4+} ions randomly distributing on 16 sites and a primitive cubic $P4_332$ space group with the two ions orderly occupying 12d and 4b sites, respectively [16, 22–25]. Moreover, the sample with Fd3m space group is widely believed to have better electrochemical performance due to the higher content of Mn^{3+} ions [22, 24, 26–28]. In our previous work [12], a thermopolymerization method was employed to synthesize

Electronic supplementary material The online version of this article (https://doi.org/10.1007/s42452-018-0069-9) contains supplementary material, which is available to authorized users.

✉ Chun-Hua Chen, cchchen@ustc.edu.cn | [1]School of Chemistry and Chemical Engineering, Heifei University of Technology, Hefei 230009, Anhui, China. [2]CAS Key Laboratory of Materials for Energy Conversions, Department of Materials Science and Engineering & Collaborative Innovation Center of Suzhou Nano Science and Technology, University of Science and Technology of China, Hefei 230026, Anhui, China.

Received: 10 September 2018 / Accepted: 19 November 2018 / Published online: 29 November 2018

the divalent-metal-ions doped samples. Among these samples, $LiNi_{0.45}Cu_{0.05}Mn_{1.5}O_4$ with $P4_332$ space group delivered excellent rate performance and good cycling stability even at elevated temperature. However, the improvement is unsatisfactory. So in this work, we aim to prepare $LiNi_{0.45}Cu_{0.05}Mn_{1.5}O_4$ with Fd3m space group and look forward to some surprises. According to literature work [16, 29–32], a high-temperature treatment (> 700 °C) can lead to the formation of disordered $LiNi_{0.5}Mn_{1.5}O_4$ with the space group Fd3m due to the release of a tiny amount of oxygen, but after the annealing treatment at 700 °C in air or oxygen for a long time, the spinel can transform its crystal structure from Fd3m to $P4_332$ space group. Such a transformation is also observed in Cu-doped composition $LiNi_{0.45}Cu_{0.05}Mn_{1.5}O_4$ [12]. Therefore, in this work, we keep the calcination process at high temperature (900 °C) to synthesize $LiNi_{0.45}Cu_{0.05}Mn_{1.5}O_4$ samples with Fd3m space group. The electrochemical testing results prove that, compared with $LiNi_{0.45}Cu_{0.05}Mn_{1.5}O_4$ with $P4_332$ space group, the disordered $LiNi_{0.45}Cu_{0.05}Mn_{1.5}O_4$ (Fd3m) exhibits excellent rate performance and cycling stability at the room temperature as well as the elevated temperature (55 °C).

2 Experimental

The $LiNi_{0.5}Mn_{1.5}O_4$ and $LiNi_{0.45}Cu_{0.05}Mn_{1.5}O_4$ samples with $P4_332$ space group were synthesized via a thermopolymerization method as described previously [12]. Lithium nitrate ($LiNO_3$, 5% excess), copper nitrate ($Cu(NO_3)_2{\cdot}3H_2O$), nickel nitrate ($Ni(NO_3)_2{\cdot}6H_2O$) and manganese acetate ($Mn(CH_3COO)_2{\cdot}4H_2O$) were mixed in stoichiometric molar ratio with 100 ml deionized water. Secondly, 50 ml acrylic acid (AA) was added to form a mixed solution, which was then kept in an oven at 150 °C for 10 h to proceed the thermopolymerization reaction and get a fluffy powder product. This powder was grinded and calcined at 500 °C for 5 h and then naturally cooled to room temperature. After another grinding, the intermediate products were further sintered at 900 °C for 15 h and subsequently annealed at 700 °C for 48 h. All these heat treatment processes were carried out in air atmosphere. For simplicity, $LiNi_{0.5}Mn_{1.5}O_4$ and $LiNi_{0.45}Cu_{0.05}Mn_{1.5}O_4$ synthesized by the above process were respectively referred to as LNM and LNM-Cu-9-7. The disordered $LiNi_{0.45}Cu_{0.05}Mn_{1.5}O_4$ materials were also prepared by a process similar to the above but without the annealing treatment at 700 °C. Therefore they were named as LNM-Cu-9.

Powder X-ray diffraction (XRD) was carried out by a diffractometer (Rigaku TTRIII, Cu K-alpha radiation) with a scanning rate of 1° min^{-1} in the range $2\theta = 10°–80°$. The morphologies of the as-prepared samples were observed under a scanning electron microscope (SEM, JSM-6390LA, JEOL). A Nicolet 8700 infrared spectrometer (Thermo Scientific Instrument Co. USA) was also used for Fourier transformed infrared (FTIR) study. An inductively coupled plasma atomic emission spectrometer (ICP) (Optima 7300 DV, Perkin-Elmer Co., USA) was introduced to measure the concentration of the soluble Mn^{2+} ions.

For electrochemical testing, the active materials (LNM, LNM-Cu-9-7 and LNM-Cu-9), acetylene black and PVDF (80:10:10, w/w/w) with *N*-methyl-2-pyrrolidone were first mixed to prepare homogenous slurries. Then they were separately dispersed on an aluminum foil with a doctor blade and dried at 70 °C overnight. The individual electrode discs with 14 mm diameter were punched out and dried at 70 °C for 2 h in a vacuum oven,and the average loading density is about 3.2 mg cm^{-2}. The CR2032 half cells were assembled in an argon-filled glove box (MBraun Labmaster 130) and the electrolyte used in the cells was 1.0 M $LiPF_6$ solution in ethylene carbonate (EC)–dimethyl carbonate (DMC) (1:1 w/w, Guotai Huarong New Chemical Materials Co.). Galvanostatic charge/discharge was carried out by a multi-channel battery cycler (Neware BTS2300, Shenzhen) with a voltage window of 3.5–4.9 V at room temperature (25 °C, RT). The cells were also cycled at 55 °C by keeping them in an oven.

The cyclic voltammetry (CV) and electrochemical impedance spectroscopy (EIS) of the cells were both conducted on a CHI 604A electrochemical instrument. The EIS tests and the CV tests were carried out in the frequency range of 0.01–10^5 Hz and in the potential window of 3.0–5.1 V at a scan rate of 0.1 mV s^{-1}, respectively. To evaluate the electrical conductivity of LNM-Cu-9 [12], the intermediate precursor of LNM-Cu-9 was pressed into discs with a diameter of 16 mm and then sintered at 900 °C for 15 h (The weight of the powder of the three samples is 1.000 g.). The sintered pellet was coated with the silver paste as conductive adhesive on top and bottom sides, then measured their size which was illustrated in Table 1 in the supporting information. Finally, they are tested on the CHI 604A electrochemical workstation.

3 Results and discussion

3.1 Crystal structures and particle morphology

The SEM images of LNM, LNM-Cu-9-7 and LNM-Cu-9 are displayed in Fig. 1. It is obvious that the particles of the

Table 1 ICP results of the dissolution of Mn^{2+} ions after 500 cycles

Samples	The dissolution of Mn (μg ml^{-1})
LNM	0.407
LNM-Cu-9-7	0.16
LNM-Cu-9	0.09

three samples own well-crystallized octahedral morphologies and similar particle size of 1–3 μm.

The XRD patterns of LNM, LNM-Cu-9-7 and LNM-Cu-9 samples are compared in Fig. 2a. All the samples reveal well-defined spinel structure without any impurities ($Li_xNi_{1-x}O$ etc.) at 37.3°, 43.3° and 63.2° [16, 22]. Rietveld refinements were performed to obtain the lattice parameter of the LNM-Cu-9 (8.1774 Å). Compared to the lattice parameter of LNM (8.1703 Å) and LNM-Cu-9-7 (8.1700 Å) [12], the slightly increased lattice parameter of LNM-Cu-9

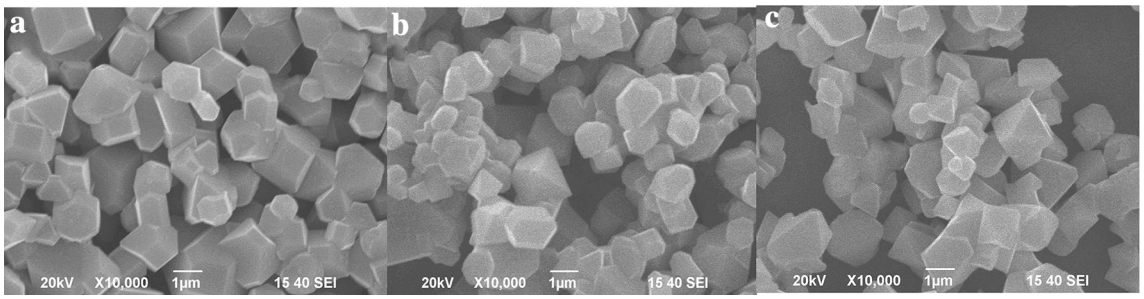

Fig. 1 SEM images of LNM (**a**), LNM-Cu-9-7 (**b**) and LNM-Cu-9 (**c**) samples

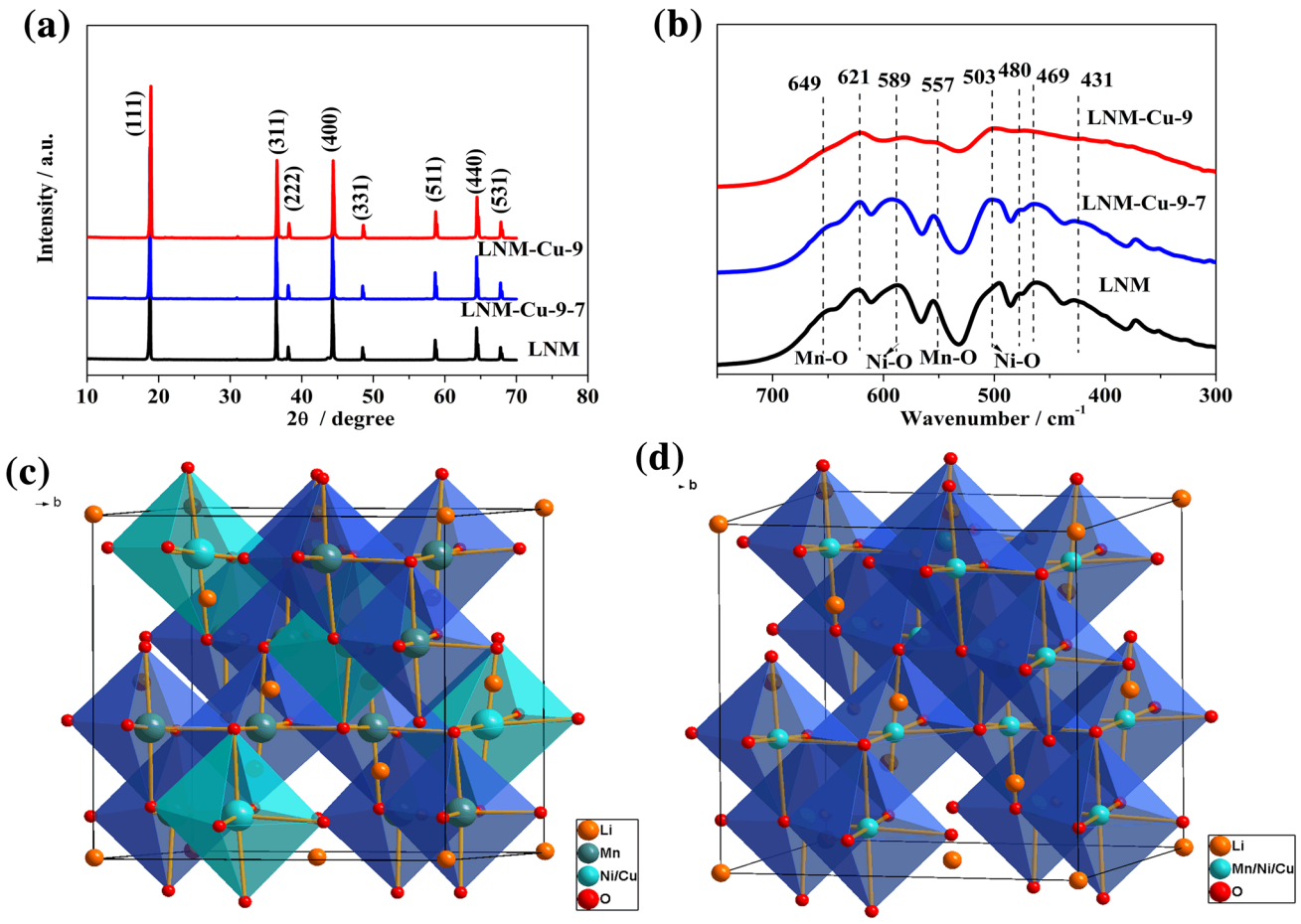

Fig. 2 XRD (**a**) patterns and FTIR spectra (**b**) of the samples: LNM, LNM-Cu-9-7 and LNM-Cu-9. Crystal structure of LNM-Cu-9-7 with $P4_332$ space group (**c**) and LNM-Cu-9 with Fd3m space group (**d**)

is due to the combined effect of the formation of Mn^{3+} (r^{3+}_{Mn} = 0.65 Å, > r^{4+}_{Mn} = 0.53 Å) and Cu^{3+} (r^{3+}_{Cu} = 0.54 Å, < r^{2+}_{Cu} = 0.73 Å) during the synthesis process.

Except for the XRD analysis, the FTIR spectra are also considered to be an effective way to distinguish the space group between Fd3m and $P4_332$. For the ordered $P4_332$ space group, there are additional three peaks separately distributed at about 646, 464 and 430 cm^{-1}, which are normally absent in the disordered Fd3m space group [33, 34]. As can be seen from Fig. 2b, LNM and LNM-Cu-9-7 samples are assigned to be the ordered $P4_332$ crystalline structure with the obvious adsorption at 649, 469 and 431 cm^{-1}. LNM-Cu-9 sample nearly has no adsorption at these three wavenumbers, suggesting that it is with disordered Fd3m space group. As shown in Fig. 2b, c, Ni^{2+}, Cu^{2+} and Mn^{4+} ions in LNM-Cu-9-7 sample with $P4_332$ space group separately occupy 4b and 12d octahedral sites. While for the LNM-Cu-9 sample with Fd3m space group, they are randomly located at the octahedral 16d sites.

3.2 Electrochemical performance at room temperature (RT)

Cyclic voltammograms for half cells of Li/LNM, Li/LNM-Cu-9-7 and Li/LNM-Cu-9 are depicted in Fig. 3. It is well known that the peaks at around 4.0 V are assigned to the redox couple Mn^{3+}/Mn^{4+} and the peaks at around 4.7 V are due to Ni^{2+}/Ni^{4+} [15–18, 35]. The weak peaks between 4.2 and 4.4 V are ascribed to the redox couple Cu^{2+}/Cu^{3+} [17, 36, 37]. As shown in Fig. 3, the voltage difference (ΔV) of the Ni^{2+}/Ni^{4+} redox peaks just as the dotted line for LNM-Cu-9 sample is smaller than the other two samples,which implying its lower polarization [17, 35, 38, 39]. There two couples of mixed valences (Cu^{2+}/Cu^{3+} and Mn^{3+}/Mn^{4+}) can be observed on the curve of LNM-Cu-9 sample, which are helpful to increase the electronic conductivity of LNM-Cu-9 sample.

The initial charge and discharge profiles and long cycling measurements are shown in Fig. 4. Figure 4a presents the initial charge/discharge profiles of LNM, LNM-Cu-9-7 and LNM-Cu-9 samples. The weak plateau at 4.2–4.4 V ascribed to the redox couple Cu^{2+}/Cu^{3+} can be observed on the charge and discharge curves of the Cu-doping LNM samples [12, 17, 18]. The voltage plateau at 4.0 V assigned to the Mn^{3+}/Mn^{4+} redox couple is only visible on the curve of LNM-Cu-9 sample, suggesting that the synthesis process without the annealing treatment leads to the formation of Mn^{3+} [15–17]. The observed charge/discharge voltage plateaus are consistent to the above CV results. The initial discharge capacity of the three samples nearly reaches 128 mAh g^{-1}. Moreover, we also have a comparison of the IR drops between the charge and discharge curves at the semi-full-charged state for the three half cells. As a result, the IR drops are 0.1 V (LNM), 0.06 V

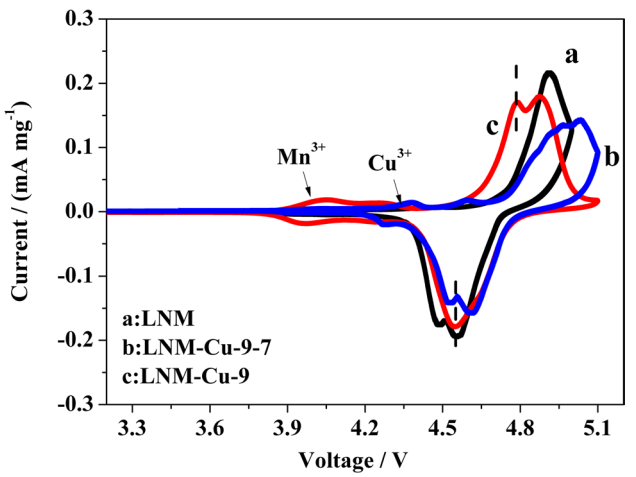

Fig. 3 CV plots of LNM (**a**), LNM-Cu-9-7 (**b**) and LNM-Cu-9 (**c**) samples between 3.0 and 5.1 V at RT

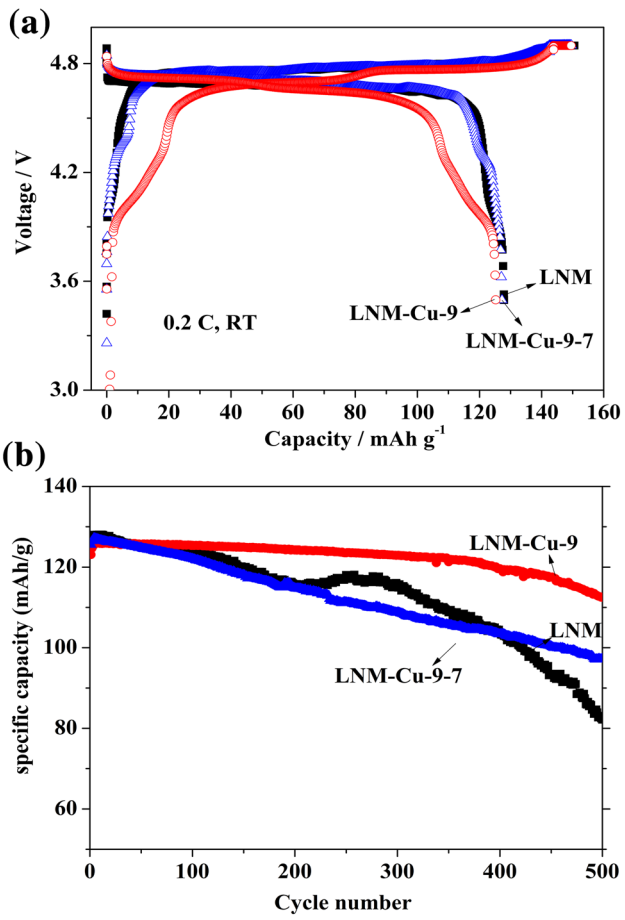

Fig. 4 The initial charge–discharge curves at 0.2 C (**a**) and cycling stability (**b**) of LNM, LNM-Cu-9-7 and LNM-Cu-9 samples at 1 C and RT

(LNM-Cu-9-7) and 0.0 V (LNM-Cu-9), respectively, which indicates the reduced polarization and impedance after Cu doping especially the Cu-doped sample with Fd3m space group. Besides, as as shown in Fig. 5b, LNM-Cu-9 exhibits much better cycling stability than LNM and LNM-Cu-9-7. LNM-Cu-9 shows a capacity retention of 100% after 300 cycles, and 91% after 500 cycles, while the capacity retentions of LNM and LNM-Cu-9-7 samples are separately 65% and 77% after 500 cycles.

After 500 cycles, the cells of Li/LNM, Li/LNM-Cu-9-7 and Li/LNM-Cu-9 are disassembled and soaked in 40 ml distilled water to measure the amounts of the dissolution of Mn^{2+} ions by ICP. The results of the dissolution of Mn^{2+} are listed in Table 1, After 500 cycles, LNM-Cu-9 exhibits the lowest amounts of soluble Mn^{2+} ions produced by the disproportionated reaction of Mn^{3+}, while the undoped LNM gives the largest dissolution of Mn^{2+} ions. Apparently, the Cu^{2+} doping can effectively prevent the dissolution of Mn^{2+} ions and this effect is more obvious with the increase of Mn^{3+} ions.

The morphologies of LNM, LNM-Cu-9-7 and LNM-Cu-9 electrodes before and after 500 cycles at RT are shown in Fig. 5. Compared to the Cu-doping samples, the surface of the LNM electrode is completely covered by the products of the side reactions occurring on the interface of the electrolyte and electrode after 500 cycles, and is partly covered for LNM-Cu-9-7 electrode. However, the particles of LNM-Cu-9 after 500 cycles are mostly exposed and remained well. The combined contribution of few soluble Mn^{2+} ions and the seldom side reaction during the repeated charge and discharge process collectively result in the excellent cycling stability of LNM-Cu-9.

To investigate the rate capability of LNM, LNM-Cu-9-7 and LNM-Cu-9, the cells were charged and discharged at the current densities from 70 mA g^{-1} (0.5 C rate) to 1400 mA g^{-1} (10 C rate). In Fig. 6a, it is obvious that LNM-Cu-9-7 and LNM-Cu-9 both deliver higher discharge capacity than LNM. Compared to LNM-Cu-9-7, LNM-Cu-9 exhibits higher discharge capacity at 8 C and 10 C, separately reaches 118.7 and 110.4 mAh g^{-1}. Also, at a current density of 1400 mA g^{-1} (10 C), as shown in Fig. 6b, the capacity retentions of LNM-Cu-9 and LNM-Cu-9-7 remain 91.2% and 80.5%, respectively after 300 cycles. Based on the above results, it can be concluded that LNM-Cu-9 owns much better electronic conductivity and cycling stability than LNM-Cu-9-7. As mentioned in Ref. [12], LNM-Cu-9-7 sample shows better electronic conductivity due to the appearance of the mixed-valence Cu^{2+}/Cu^{3+} couple and the mixed-valence couple facilitating electron hopping has been reported in literatures [18, 22]. Hence, for LNM-Cu-9, the additional mixed-valence Mn^{3+}/Mn^{4+} can further improves the electronic conductivity, which results in much better rate performance than LNM-Cu-9-7.

EIS measurements are adopted to test the half-cells of Li/LNM, Li/LNM-Cu-9-7 and Li/LNM-Cu-9 at the state-of-charge (SOC) of 50%. The EIS spectra, the equivalent circuit and the fitting results are shown in Fig. 7. In the equivalent circuit, R_1 is ascribed to the ohmic resistance and R_2 is assigned to the charge transfer resistance at the interface between the electrode and the electrolyte. Based on the

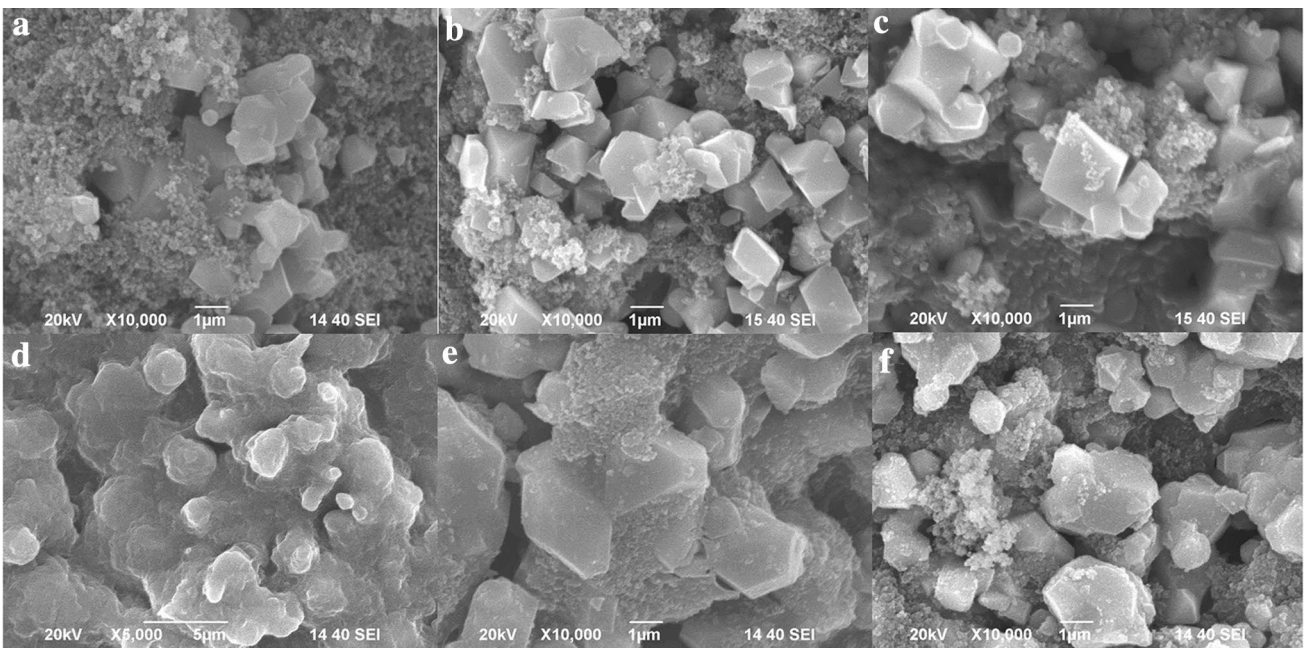

Fig. 5 SEM images of the electrodes before and after 500 cycles: LNM (**a**, **d**), LNM-Cu-9-7 (**b**, **e**) and LNM-Cu-9 (**c**, **f**) samples

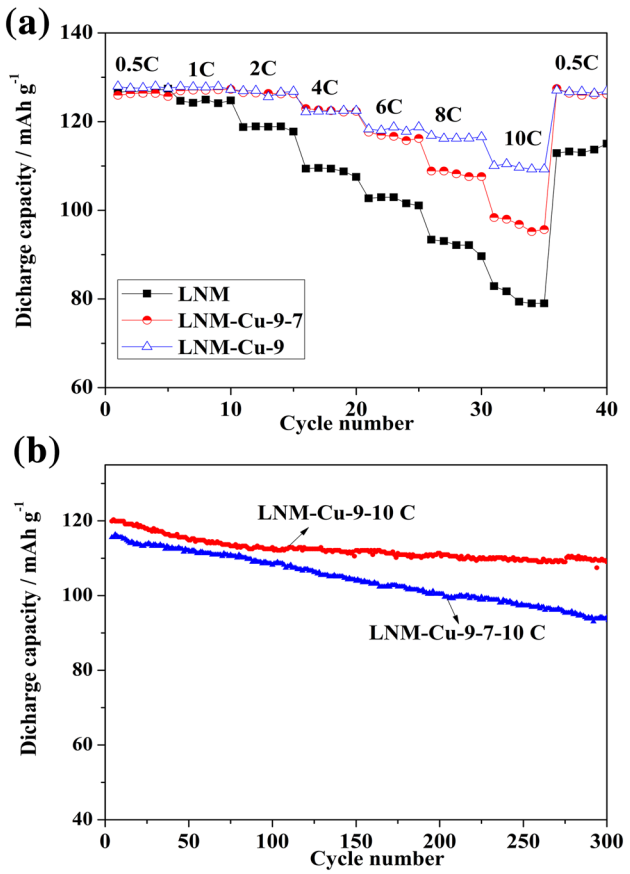

Fig. 6 The rate performance (**a**) at different current densities of LNM, LNM-Cu-9-7 and LNM-Cu-9 samples at RT. The cycling stability of the Cu-doping samples at a large current density 1400 mA g^{-1} (**b**)

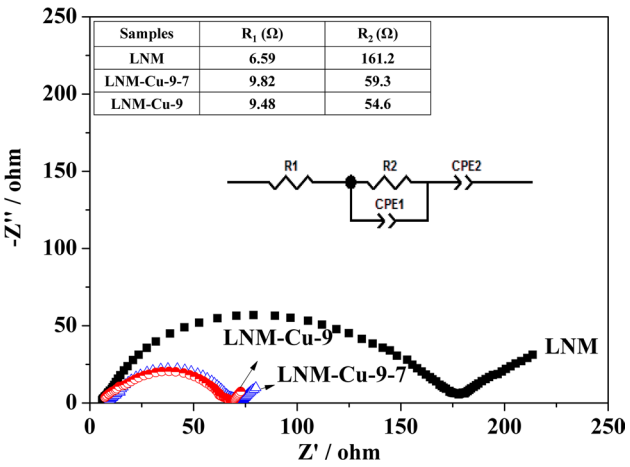

Fig. 7 EIS spectra of Li/LNM, Li/LNM-Cu-9-7 and Li/LNM-Cu-9 half-cells at RT

fitting results shown in the inserted table in Fig. 7, LNM possesses the largest R_2 (161.2 Ω), while LNM-Cu-9-7 and LNM-Cu-9 own smaller R_2 (59.3 Ω and 54.6 Ω, respectively),

Table 2 The electrical conductivity of LNM, LNM-Cu-9-7, and LNM-Cu-9 samples at RT

Samples	Resistance (Ω)	Electrical conductivity (S cm^{-1})
LNM	1.05×10^{6}	1.53×10^{-7}
LNM-Cu-9-7	2.62×10^{4}	4.54×10^{-6}
LNM-Cu-9	1.78×10^{3}	3.58×10^{-5}

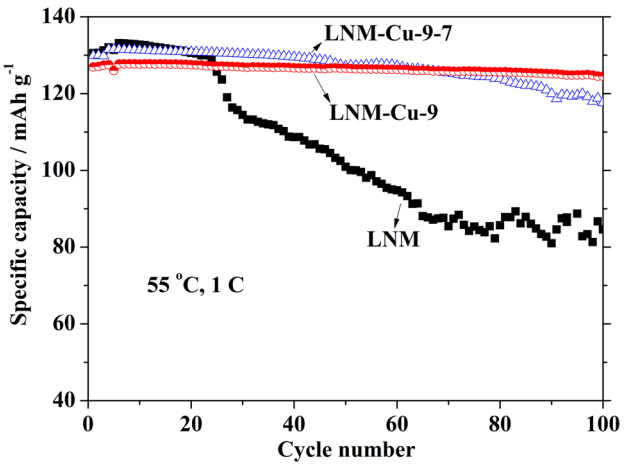

Fig. 8 The electrochemical cycling performances of LNM, LNM-Cu-9-7 and LNM-Cu-9 at 55 °C and 1 C

which are just consistent with their rate performances in Fig. 6a.

Meanwhile, the electrical conductivities of LNM, LNM-Cu-9-7 and LNM-Cu-9 are also measured based on the EIS measurement of their sintered pellets (Fig. S1). The results are listed in Table 2. Undoubtedly, LNM-Cu-9 has the highest electrical conductivity (3.58×10^{-5} S cm^{-1}) which is due to the existences of mixed-valences Cu^{2+}/Cu^{3+} and Mn^{3+}/Mn^{4+} couples, which is consistent to its best rate performance shown in Fig. 6.

3.3 Cycling behavior of LNM, LNM-Cu-9-7 and LNM-Cu-9 at 55 °C

Figure 8 shows the electrochemical performances of LNM, LNM-Cu-9-7 and LNM-Cu-9 at 55 °C. It is noticed that the Cu-doping samples both exhibit better cycling stability than LNM sample at the elevated temperature (55 °C). Moreover, the discharge capacity of LNM-Cu-9 has nearly no capacity loss after 100 cycles, i.e. with a capacity retention of 100%. Thus LNM-Cu-9 shows outstanding cycling stability at 55 °C. Therefore, LNM-Cu-9 surely further improves the electrochemical performance at room

Table 3 Comparison of the electrochemical performance for the divalent-cation-doped $LiNi_{0.5}Mn_{1.5}O_4$ spinel with our sample

Samples	Synthesis method	Space group	Rate performance (mAh g^{-1})	Capacity fading (% percycle)	References
$LiNi_{0.47}Mg_{0.03}Mn_{1.5}O_4$	Sol–gel	–	74@5C, 106@0.2C	–	[40]
Mg(GD)-LNM	Coprecipitaion	Fd3m	91@5C, 121@0.1C	0.1% (RT, 0.5C), 0.4% (55 °C, 0.5C)	[41]
$LiNi_{0.4}Mg_{0.1}Mn_{1.5}O_4$	Coprecipitaion	Fd3m	35@5C, 99@0.5C	0.02% (RT, 0.5C)	[19]
$LiNi_{0.4}Cu_{0.1}Mn_{1.5}O_4$	Coprecipitaion	Fd3m	70@5C, 106@0.5C	0.08% RT, 0.5C)	[19]
$LiNi_{0.42}Cu_{0.08}Mn_{1.5}O_4$	Coprecipitaion	$P4_332$	115@10C, 121@0.2C	0.08% (RT, 0.5C)	[18]
$LiNi_{0.45}Cu_{0.05}Mn_{1.5}O_4$	Sol–gel	Fdm	85@0.5C, 120@0.05C	–	[42]
$LiNi_{0.45}Cu_{0.05}Mn_{1.5}O_4$	Sol–gel	$P4_332$	97@5C, 130@0.5C	–	[17]
$LiNi_{0.45}Mg_{0.05}Mn_{1.5}O_4$	Spray pyrolysis	$P4_332$	115@0.1C	0.06% (RT, 1C), 0.14% (60 °C, 1C)	[43]
$LiNi_{0.45}Cu_{0.05}Mn_{1.5}O_4$	Thermo-polymerization	$P4_332$	98@10C, 128@0.2C	0.03% (RT, 1C)	[12]
$LiNi_{0.45}Mg_{0.05}Mn_{1.5}O_4$	Thermo-polymerization	$P4_332$	92@10C, 123@0.2C	0.03% (RT, 1C)	[12]
$LiNi_{0.45}Cu_{0.05}Mn_{1.5}O_4$	Thermo-polymerization	Fd3m	110@10C, 128@0.2C	0.03% (RT, 1C)	This work

temperature and the elevated temperature, which just realizes our anticipated objective in the beginning.

Finally, Table 3 compares the electrochemical performance of LNM-Cu-9 with those of other $LiNi_{0.5}Mn_{1.5}O_4$ samples reported in literature. Undoubtedly, LNM-Cu-9 sample shows superior electrochemical properties both in cycling stability and rate capability.

4 Conclusion

In summary, the results of physical properties analysis demonstrate that LNM-Cu-9 sample without the annealing treatment at 700 °C is indeed with the disordered Fd3m space group. During the electrochemical measurements, LNM-Cu-9 sample delivers the initial discharge capacity 127.2 mAh g^{-1} and the capacity retention 91% after 500 cycles at RT. Moreover, at the elevated temperature (55 °C), the capacity retention can keep 100% after 100 cycles. Besides, due to it high electrical conductivity (3.58×10^{-5} S cm^{-1}), LNM-Cu-9 sample exhibits the discharge capacity 110.4 mAh g^{-1} at the large current density (10 C rate). The LNM-Cu-9 cathode material with outstanding rate capability and cycling stability at the room and elevated temperature, is anticipated to provide new opportunities for the high power and high energy density LIBs in the commercial applications.

Acknowledgements This work was supported by National Key R&D Program of China (Grant No. 2018YFB0905400) and National Science Foundation of China (NSAF U1630106, Grant No. 51577175). We are also grateful to Elementec Ltd in Suzhou for its technical support.

Compliance with ethical standards

Conflict of interest The authors declare that they have no competing interests.

References

1. Acrio AS, Bruce P, Scrosati B, Tarascon JM, Schalkwijk WV (2005) Nanostructured materials for advanced energy conversion and storage devices. Nat Mater 4:366–377
2. Amin R, Belharouk I (2017) Part I: electronic and ionic transport properties of the ordered and disordered $LiNi_{0.5}Mn_{1.5}O_4$ spinel cathode. J Power Sour 348:311–317
3. Jia GL, Jiao CM, Xue WJ, Zheng SH, Wang J (2016) Improvement in electrochemical performance of calcined $LiNi_{0.5}Mn_{1.5}O_4$/GO. Solid State Ion 292:15–21
4. Sun P, Ma Y, Zhai TY, Li HQ (2016) High performance $LiNi_{0.5}Mn_{1.5}O_4$ cathode by Al-coating and Al^{3+}-doping through a physical vapor deposition method. Electrochim Acta 191:237–246
5. Moorhead-Rosenberg Z, Huq A, Goodenough JB, Manthiram A (2015) Electronic and electrochemical properties of $Li_{1-x}Mn_{1.5}Ni_{0.5}O_4$ spinel cathodes as a function of lithium content and cation ordering. Chem Mater 27:6934–6945
6. Wu QL, Liu YZ, Johnson CS, Li YX, Dees DW, Lu WQ (2014) Insight into the structural evolution of a high-voltage spinel for lithium-ion batteries. Chem Mater 26:4750–4756
7. Lin MX, Ben LB, Sun Y (2015) Insight into the atomic structure of high-voltage spinel $LiNi_{0.5}Mn_{1.5}O_4$ cathode material in the first cycle. Chem Mater 27:292–303
8. Ma J, Hu P, Cui GL, Chen LQ (2016) Surface and interface issues in spinel $LiNi_{0.5}Mn_{1.5}O_4$: insights into a potential cathode material for high energy density lithium ion batteries. Chem Mater 28:3578–3606
9. Zhu YR, Yi TF, Zhu RS (2013) Increased cycling stability of $Li_4Ti_5O_{12}$-coated $LiNi_{0.5}Mn_{1.5}O_4$ as cathode material for lithium-ion batteries. Ceram Int 39:3087–3094

10. Liu GQ, Zhang JY, Zhang XH (2017) Study on oxygen deficiency in spinel $LiNi_{0.5}Mn_{1.5}O_4$ and its Fe and Cr-doped compounds. J Alloys Compd 725:580–586
11. Deng JC, Xu YL, Xiong LL (2016) Improving the fast discharge performance of high-voltage $LiNi_{0.5}Mn_{1.5}O_4$ spinel by Cu^{2+}, Al^{3+}, Ti^{4+} tri-doping. J Alloys Compd 677:18–26
12. Deng MM, Zou BK, Shao Y (2017) Comparative study of the electrochemical properties of $LiNi_{0.5}Mn_{1.5}O_4$ doped by bivalent ions (Cu^{2+}, Mg^{2+}, and Zn^{2+}). J Solid State Chem 21:1733–1742
13. Lin M, Wang SH, Gong ZL (2013) A strategy to improve cyclic performance of $LiNi_{0.5}Mn_{1.5}O_4$ in a wide voltage region by Ti-doping. J Electrochem Soc 160:3036–3040
14. Xin Q, Berislav B, Aurelien DP (2015) Influence of thermal treated carbon black conductive additive on the performance of high voltage spinel Cr-doped $LiNi_{0.5}Mn_{1.5}O_4$ composite cathode electrode. J Electrochem Soc 162:339–343
15. Zhong GB, Wang YY, Zhang ZC (2011) Effects of Al substitution for Ni and Mn on the electrochemical properties of $LiNi_{0.5}Mn_{1.5}O_4$. Electrochim Acta 56:6554–6561
16. Zhong GB, Wang YY, Yu YQ (2012) Electrochemical investigations of the $LiNi_{0.45}M_{0.10}Mn_{1.45}O_4$ (M = Fe Co, Cr) 5 V cathode materials for lithium ion batteries. J Power Sour 205:385–393
17. Sha O, Qiao Z, Wang SL, Tang ZY (2013) Improvement of cycle stability at elevated temperature and high rate for $LiNi_{0.5-x}Cu_xMn_{1.5}O_4$ cathode material after Cu substitution. Mate Res Bull 48:1606–1611
18. Chemelewski KR, Manthiram A (2013) Origin of site disorder and oxygen nonstoichiometry in $LiMn_{1.5}Ni_{0.5-x}M_xO_4$ (M = Cu and Zn) cathodes with divalent dopant ions. J Phys Chem C 117:12465–12471
19. Zhu W, Liu D, Trottier J (2014) Comparative studies of the phase evolution in M-doped $Li_xMn_{1.5}Ni_{0.5}O_4$ (M = Co, Al, Cu and Mg) by in situ X-ray diffraction. J Power Sour 264:290–298
20. Yi TF, Xie Y, Zhu YR (2012) High rate micron-sized niobium-doped $LiMn_{1.5}Ni_{0.5}O_4$ as ultra high power positive-electrode material for lithium-ion batteries. J Power Sour 211:59–65
21. Kiziltas-Yavuz N, Bhaskar A, Dixon D (2014) Improving the rate capability of high voltage lithium-ion battery cathode material $LiMn_{1.5}Ni_{0.5}O_4$ by ruthenium doping. J Power Sour 267:533–541
22. Haridas AK, Sharma CS, Rao TN (2016) Caterpillar-like submicron $LiMn_{1.5}Ni_{0.5}O_4$ structures with site disorder and excess Mn^{3+} as high performance cathode material for lithium ion batteries. Electrochim Acta 212:500–509
23. Kim JH, Myung ST, Yoon CS (2004) Comparative study of $LiMn_{1.5}Ni_{0.5}O_{4-\delta}$ and $LiMn_{1.5}Ni_{0.5}O_4$ cathodes having two crystallographic structures: Fd3m and $P4_332$. Chem Mater 16:906–914
24. Gu YJ, Li Y, Chen YB (2016) Comparison of Li/Ni antisite defects in Fd3m and $P4_332$ nanostructured $LiMn_{1.5}Ni_{0.5}O_4$ electrode for Li-ion batteries. Electrochim Acta 213:368–374
25. Rosedhi ND, Idris NH, Rahman MM (2016) Disordered spinel $LiMn_{1.5}Ni_{0.5}O_4$ cathode with improved rate performance for lithium-ion batteries. Electrochim Acta 206:374–380
26. Jafta CJ, Mathe MK, Manyala N (2013) Microwave-assisted synthesis of high-voltage nanostructured $LiMn_{1.5}Ni_{0.5}O_4$ spinel: tuning the Mn^{3+} content and electrochemical performance. ACS Appl Mater Interfaces 5:7592–7598
27. Chong J, Xun SD, Song XY (2013) Surface stabilized $LiMn_{1.5}Ni_{0.5}O_4$ cathode materials with high-rate capability and long cycle life for lithium ion batteries. Nano Energy 2:283–293
28. Ariyoshi K, Iwakoshi Y, Nakayama N (2014) Topotactic two-phase reactions of $Li[Ni_{1/2}Mn_{3/2}]O_4$ ($P4_332$) in nanoqueous lithium cells. J Electrochem Soc 151:296–303
29. Kunduraci M, Amatucci GG (2006) Synthesis and characterization of nanostructured 4.7 V $Li_xMn_{1.5}Ni_{0.5}O_4$ spinels for high-power lithiun-ion batteries. J Electrochem Soc 153:1345–1352
30. Ohzuku T, Ariyoshi K, Yamamoto S (2002) Synthesis and characterization of $Li[Ni_{1/2}Mn_{3/2}]O_4$ by two-step solid state reaction. J Ceram Soc Jpn 110:501–505
31. Kim J, Chi M, Pieczonka NPW (2014) Integrated nanodomains disordered and ordered spinel phases in $LiNi_{0.5}Mn_{1.5}O_4$ for Li-ion batteries. Chem Mater 26:4377–4386
32. Xiao J, Chen X, Sushko PV (2012) High-performance spinel $LiNi_{0.5}Mn_{1.5}O_4$ controlled by Mn^{3+} concentration and site disorder. Adv Mater 24:2109–2116
33. Alcantara R, Jaraba M, Lavela P (2004) Changes in the local structure of $LiMg_yNi_{0.5-y}Mn_{1.5}O_4$ electrode materials during lithium extraction. Chem Mater 16:1573–1579
34. Kunduraci M, Al-Sharab JF, Amatucci GG (2006) High-power nanostructured $LiMn_{2-x}Ni_xO_4$ high-voltage lithium-ion battery electrode materials: electrochemical impact of electronic conductivity and morphology. Chem Mater 18:3585–3592
35. Wang HL, Shi ZQ, Li JW (2015) Direct carbon coating at high temperature on $LiNi_{0.5}Mn_{1.5}O_4$ cathode: unexpected influence on crystal structure and electrochemical performances. J Power Sour 288:206–213
36. Yang MC, Xu B, Cheng JH, Pan CJ, Hwang BJ, Meng YS (2011) Electronic, structural, and electrochemical properties of $LiNi_xCu_yMn_{2-x-y}O_4$ ($0 < x < 0.5$, $0 < y < 0.5$) high-voltage spinel materials. Chem Mater 23:2832–2881
37. Fang X, Shen CF, Ge MY (2015) High-power lithium ion batteries based on flexible and light-weight cathode of $LiNi_{0.5}Mn_{1.5}O_4$/carbon nanotube film. Nano Energy 12:43–51
38. Wang HL, Tan TA, Yang P (2011) High-rate performances of the Ru-doped spinel $LiNi_{0.5}Mn_{1.5}O_4$: effects of doping and particle size. J Phys Chem C 115:6102–6110
39. Liu J, Manthiram A (2009) Understanding the improved electrochemical performances of Fe-substituted 5 V spinel cathode $LiNi_{0.5}Mn_{1.5}O_4$. J Phys Chem C 113:15073–15079
40. Locati C, Lafont U, Simonin L, Ooms F, Kelder EM (2007) Mg-doped $LiNi_{0.5}Mn_{1.5}O_4$ spinel for cathode materials. J Power Sour 174:847–851
41. Liu MH, Huang HT, Lin CM, Chen JM, Liao SC (2014) Mg gradient-doped $LiNi_{0.5}Mn_{1.5}O_4$ as the cathode material for Li-ion batteries. Electrochim Acta 120:133–139
42. Ein-Eli Y, Vaughey JT, Thackeray MM (1999) $LiNi_xCu_{0.5-x}Mn_{1.5}O_4$ spinel electrodes, superior high-potential cathode materials for Li batteries I. Electrochemical and structural studies. J Electrochem Soc 146:908–913
43. Shiu JJ, Pang WK, Wu SH (2013) Preparation and characterization of spinel $LiNi_{0.5-x}Mg_xMn_{1.5}O_4$ cathode materials via spray pyrolysis method. J Power Sour 244:35–42